

Simultaneous reconstruction and registration algorithm for limited view transmission tomography using a single bivariate Gaussian approximation to the joint histogram

Dominique Van de Sompel^a, Andrew McLennan^a and Michael Brady^{a*}

^aUniversity of Oxford, Department of Engineering Science,
Parks Road, Oxford OX1 3PJ, UK,

Abstract. We develop a novel simultaneous reconstruction and registration algorithm for limited view transmission tomography. The method is formulated as an optimization problem using Bayesian probability theory. Results show a promising mitigation of the data insufficiency problem in limited view tomography. To our knowledge, this is the first study to incorporate non-registered, multimodal anatomical priors into limited view transmission tomography.

1 Introduction

Limited view transmission tomography is widely used in industrial as well as clinical applications, where it is commonly motivated by geometric design constraints on the imaging machinery, limitations on time for image acquisition, and/or efforts to reduce patient radiation dose. Common clinical applications include intra-operative imaging for reference with a pre-operative planning CT, angiography, chest tomosynthesis, dental tomosynthesis, cardiac CT, and orthopaedic imaging [1]. However, limited view transmission tomography suffers from the limitation that its reconstructions are fundamentally underdefined. The data insufficiency problem can be understood in terms of the Fourier Slice Theorem [2]. This theorem states that the Fourier transform of a parallel projection of an image f gives a slice through its Fourier domain F perpendicular to the direction of the projection. Hence the incomplete angular sampling of limited view tomography leaves large swathes of the Fourier space unmeasured. In this work, we estimate the unsampled information by incorporating an anatomical prior into the reconstruction process. Our intention is to eventually use this approach to regularize limited view x-ray tomography using MRI priors (eg. regularizing digital breast tomosynthesis using an MR scan of the same patient).

The use of anatomical priors has been considered previously in emission as well as transmission tomography, where the majority of studies have focused on intensity difference based similarity metrics for monomodal regularization. Examples include the incorporation of planning CTs to regularize intraoperative tomosynthesis reconstructions [3] in transmission tomography, and the simulation of template PET volumes from CT or MRI priors [4] in emission tomography. In these studies it was assumed that the anatomical prior and the object to be reconstructed were aligned *a priori*. Furthermore, only a few studies have investigated the use of information theoretic similarity measures such as mutual information [5] and joint entropy [6,7] for multimodal regularization, and this only in the field of emission tomography. Mutual information was considered first due to its success in image registration, but it was later demonstrated by Nuyts [6] that joint entropy introduces less bias into the reconstruction and may therefore be more appropriate. In our previous work [8], we built on Nuyts' results and applied joint entropy (JE) regularization to limited view transmission tomography with *a priori* registered anatomical priors. To our knowledge, this was the first study to do so. We also identified JE's vulnerability to local optima when used in limited view tomography and proposed a novel approximation to increase robustness. This consisted of approximating the joint histogram by its first and second moments. As was shown, this approximation gives good results when the joint histogram is bimodal or contains multiple clusters that are roughly aligned. In this work, we extend our method to a simultaneous reconstruction and registration algorithm, which can accommodate anatomical priors that are not registered *a priori*. To our knowledge, the incorporation of non-registered, multimodal anatomical priors has not been attempted previously in limited view transmission tomography.

*Corresponding author: Dominique Van de Sompel. Email: dominique.vandesompel@stx.ox.ac.uk.

2 Methods

2.1 Objective function

The SRR algorithm is formulated as an optimization problem. Our objective is to maximize the joint posterior probability $P(x, \delta|r, B)$, where x is the attenuation map of the imaged object, δ is the deformation field, r is the observed projection data (photon counts), and B is the anatomical prior image. Using Bayes' rule and the definition of conditional probability, the posterior probability can be decomposed as

$$P(x, \delta|r, B) = \frac{1}{Z} P(r|x) P(B|x, \delta) P(x) P(\delta) \quad (1)$$

where we have assumed a uniform prior distribution for the projection data r , and that the marginal probabilities of x and δ are independent. Note also that $P(r|B, x, \delta) = P(r|x)$ since the projection data depends only on the object's attenuation map. After log transformation, dropping constant terms, and adding hyperparameters to control the strength of each term, we obtain the general objective function

$$\psi(x, \delta) = \log P(r|x) + \beta \log P(B|x, \delta) + \gamma \log P(x) + \omega \log P(\delta) \quad (2)$$

The probability $P(r|x)$ is the standard Poisson data likelihood, the probability $P(B|x, \delta)$ relates the registration to the ongoing reconstruction, and the probabilities $P(x)$ and $P(\delta)$ give the marginal probability distributions of the attenuation map and deformation field, respectively. In this work, we model the deformation field δ using a coarse sub-grid of B-splines. The data likelihood term, then, can be expressed as a sum of concave functions $h_i(l_i)$:

$$\log P(r|x) = \sum_{i=1}^M h_i(l_i) + \text{constant} \quad (3)$$

where $h_i(l_i) = -(r_{0,i}e^{-l_i} + b_i) + r_i \log(r_{0,i}e^{-l_i} + b_i)$, and where $l_i = \sum_{j=1}^N a_{ij}x_j$. The N -dimensional vector x is the attenuation map of the object, a_{ij} is the length of traversal of the i^{th} ray through the j^{th} pixel, r_i is the photon count observed by the i^{th} detector, $r_{0,i}$ is the number of photons leaving the source for the i^{th} ray, and b_i accounts for scatter events. Next, the term $\log P(B|x, \delta)$ quantifies the similarity between the reconstruction and the anatomical prior. Many similarity metrics have been proposed in the registration literature, providing us with a wide range of choices. Initially, we explored the suitability of joint entropy and mutual information for use in the SRR algorithm. However, it was found that, despite their success in image registration, their behavior as image regularizers in limited view transmission tomography is poor or even undesirable [6, 8]. In this work, we continue to use standard similarity metrics in the registration component of our algorithm (i.e. when updating δ), but switch to a similarity metric that has a more desirable performance and is easier to optimize in x . For the registration component, we use normalized mutual information (NMI), which allows for anatomical priors from different imaging modalities. For the updates of x , we use an approximate similarity metric that mimicks the cluster-narrowing effect of information theoretic measures in the joint histogram, yet is easier to handle and yields more desirable results. The specific approximation is to minimize the joint entropy of a single Gaussian approximation to the joint histogram. In other words, we let

$$P(B|x, \delta) = \frac{1}{Z_B} \exp(-H_{SG}) \quad (4)$$

where Z_B is a normalization constant, and H_{SG} denotes the joint entropy of the single Gaussian approximation to the joint histogram of x and B . The advantage of this similarity metric is that it yields a quadratic function in x , and hence enables relatively cheap update steps and fast convergence rates in x when used in combination with the globally concave data likelihood term. We have previously reported that the proposed similarity metric performs best for cases where the ground truth joint histogram shows two dominant clusters, or multiple ones that are more or less aligned [8]. This was verified using pre-registered priors. Let us now derive the form of H_{SG} . The single Gaussian approximation can be derived by viewing the joint histogram as the sum of N bivariate Gaussians, where N is again the number of pixels in the attenuation map. To

approximate this Gaussian mixture model by a single bivariate Gaussian of the same first and second moments, we use the expressions $\mu^* = \frac{1}{N} \sum_{j=1}^N \mu_j$ and $\Sigma^* = \frac{1}{N} \sum_{j=1}^N (\Sigma_j + \mu_j \mu_j^T) - \mu^* \mu^{*T}$, where $\mu_j = \begin{bmatrix} x_j \\ B_j^* \end{bmatrix}$, and $\Sigma_j = \begin{bmatrix} \sigma^2 & 0 \\ 0 & \sigma^2 \end{bmatrix}$. The notation B_j^* is shorthand for $B(\rho_j + \delta_j)$, where ρ_j is the coordinate of the source pixel x_j , and δ_j is the displacement vector at that source pixel (see also Section 2.2.2). In other words, B_j^* is the intensity of the prior B at the point corresponding to x_j , as given by the current estimate of δ . The interpolation of the prior B can be achieved using many different methods, such as linear, quadratic, cubic or B-spline interpolation. In this study we have used quadratic interpolation as a compromise between accuracy and ease of implementation. The entropy of the fitted single Gaussian, then, is given by $H_{SG} = \frac{1}{2} \ln((2\pi e)^2 |\Sigma^*|)$. From this expression, we can see that the joint entropy of the single Gaussian can be minimized simply by minimizing the variance $|\Sigma^*|$. After substituting in the relevant expressions and dropping constant terms, $|\Sigma^*|$ reduces to the penalty function $R(x, \delta) = - \left[C_B C_x - \left(\frac{1}{N} \sum_{j=1}^N x_j B_j^* - c_B c_x \right)^2 \right]$, where the variables c_B, C_B, c_x and C_x are defined as $c_B = \frac{1}{N} \sum_{j=1}^N B_j^*$, $c_x = \frac{1}{N} \sum_{j=1}^N x_j$, $C_B = \sigma^2 + \frac{1}{N} \sum_{j=1}^N B_j^{*2} - c_B^2$ and $C_x = \sigma^2 + \frac{1}{N} \sum_{j=1}^N x_j^2 - c_x^2$.

Next, we assume a uniform distribution for the marginal probability $P(x)$, allowing us to focus instead on the adequacy of the similarity term to regularize the reconstruction. If needed, however, it would be straightforward to impose spatial coherence constraints in the form of Markov Random Field (MRF) distributions by defining concave penalty functions (such as quadratic or edge-preserving Huber functions) over nearest-neighbor cliques. This would also preserve the global concavity of the objective function in x . Finally, to achieve spatial smoothness for the deformation field δ , we use a MRF prior defined as

$$P(\delta) = \frac{1}{Z_\delta} \exp \left[- \sum_p \sum_{n \in \mathcal{N}_p} w_{pn} \left[\phi(\delta_{p,x} - \delta_{n,x}) + \phi(\delta_{p,y} - \delta_{n,y}) \right] \right] \quad (5)$$

where Z_δ is a normalization constant, the integer p indexes the control points, and \mathcal{N}_p represents the neighborhood centered on the p^{th} control point. The concave function $\phi(t)$ penalizes the difference between adjacent $\delta_{p,x}$ and $\delta_{p,y}$ entries, and the weights w_{pn} represent the clique weights. Here we use a quadratic function for $\phi(t)$, though the extension to edge-preserving penalty functions is trivial.

2.2 Optimization

To optimize the objective function, we alternate between updates of x and δ , each time keeping the other constant. In other words, we alternate between reconstructing the attenuation map and registering it with the anatomical prior. The optimization steps used are explained next.

2.2.1 x -update (reconstruction)

Keeping δ constant, and assuming a uniform distribution for $P(x)$, the objective function reduces to $\psi(x) = \log P(r|x) + \beta \log P(B|x, \delta) = \sum_{i=1}^M h_i(l_i) + \beta R(x, \delta)$. The data likelihood term $P(r|x)$ can be minorized by parabolas of an optimal curvature [9]. This gives

$$Q(x; x^n) = \sum_{i=1}^M q_i(l_i; l_i^n) + \beta R(x, \delta) \leq \sum_{i=1}^M h_i(l_i) + \beta R(x, \delta) \quad (6)$$

where $q_i(l_i; l_i^n) = h_i(l_i^n) + \dot{h}_i(l_i^n)(l_i - l_i^n) + \frac{1}{2} c_i(l_i^n)(l_i - l_i^n)^2$, and x^n denotes the image estimate at the beginning of the n^{th} iteration. The optimal curvatures were given by Erdogan and Fessler [9] as

$$c_i(l_i^n) = \begin{cases} \left[2 \frac{h_i(0) - h_i(l_i^n) + \dot{h}_i(l_i^n) l_i^n}{(l_i^n)^2} \right]_-, & l_i^n > 0 \\ \left[\ddot{h}_i(0) \right]_-, & l_i^n = 0, \end{cases} \quad (7)$$

which yields a parabola tangent at l_i^n that intersects the original h_i function at $l_i = 0$. Since the surrogate $Q(x; x^n)$ in Eqn. 6 is globally concave and quadratic, we can optimize it efficiently using a Newton-Raphson steepest ascent scheme. The direction of steepest ascent at the n^{th} iterate $x = x^n$ is given by

$$x'_j = \sum_{i=1}^M \dot{h}_i(l_i) a_{ij} - \beta \left\{ \frac{2C_B^n}{N} [x_j^n - c_x^n] - \frac{2}{N} \left(\frac{1}{N} \sum_{j=1}^N x_j^n B_j^{*n} - c_B^n c_x^n \right) (B_j^{*n} - c_B^n) \right\} \quad (8)$$

By parameterizing the image x as $x = x^n + \lambda x'$, where x' represents the search direction, we can solve for the optimum of the surrogate along that direction analytically. The solution can be found to be $\lambda_{opt} = \frac{-V}{W}$, where

$$V = \sum_{i=1}^M \dot{h}_i(l_i^n) \left(\sum_{j=1}^N a_{ij} x'_j \right) - \beta \frac{2M'}{N} \left(\sum_{j=1}^N x_j^n x'_j - \frac{1}{N} \sum_{j=1}^N x_j^n \sum_{j=1}^N x'_j \right) + \beta \frac{2}{N^2} \left(\sum_{j=1}^N x_j^n B_j - m \sum_{j=1}^N x_j^n \right) \left(\sum_{j=1}^N x'_j B_j - m \sum_{j=1}^N x'_j \right) \quad (9)$$

and

$$W = \sum_{i=1}^M c_i \left(\sum_{j=1}^N a_{ij} x'_j \right)^2 - \beta \frac{2M'}{N} \left(\sum_{j=1}^N x_j'^2 - \frac{1}{N} \left(\sum_{j=1}^N x'_j \right)^2 \right) + \beta \frac{2}{N^2} \left(\sum_{j=1}^N x'_j B_j - m \sum_{j=1}^N x'_j \right)^2 \quad (10)$$

2.2.2 δ -update (registration)

Keeping x constant, the objective function reduces to $\psi(x) = \beta \log P(B|x, \delta) + \omega \log P(\delta)$. In this work, we define x to be the source image, and B to be the target image. In other words, we define the control point grid on the image x rather than the prior B . This makes the reconstruction step easier since the data likelihood term is defined in terms of the pixel centers x_j , and not values in between. If the correspondence map were to link values of B to values of x_j that lie in between the regular pixel grid, we would need to consider details of the image interpolation model when computing the updates for x_j . Initially we used a dense deformation field model for δ (i.e. every source pixel x_j acts as a control point). Using a quadratic image interpolation model, we found that the cost function $\psi(\delta)$ was locally a fourth order polynomial along the direction of steepest ascent (derivation not reproduced here). However, as with any dense formulation, the optimization showed a slow convergence rate, and sensitivity to local optima. Hence we switched to an off-the-shelf implementation provided by Glocker [10]¹, which uses the fastPD algorithm to optimize MRF-formulated registration metrics using a B-spline deformation model. This implementation provides a range of similarity metrics, of which we focused on the NMI metric. We note here that preliminary experiments using the normalized cross-correlation (NCC) similarity metric seemed promising as well.

3 Results and Discussion

Here we compare the performance of the SRR algorithm to that of the unregularized maximum likelihood (ML) algorithm. Fig. 1 illustrates the results for two different phantoms, where we have reconstructed unknown attenuation maps from 16 simulated projections distributed evenly over $\pm 30^\circ$ and an unregistered multimodal anatomical prior. The ground truth attenuation maps shown in Fig. 1 were of course not supplied to the reconstruction algorithm. The image size was 200x200 for all examples. The results show a greatly increased accuracy of reconstruction, particularly so for smaller features of the image (such as the blobs in the blob phantom). The number of steepest ascent updates used for every reconstruction step was 50, giving a run time of approximately 2 seconds per x -update. The registration step consisted of 5 iterations of Ben Glocker's fastPD algorithm, which completed in approximately 1 second. Hence the run time per total iteration of the SRR algorithm was approximately 3 seconds. The total number of iterations required to reach convergence ranged between 2 for the blob phantom, and 5 for the ideal breast phantom.

¹A GUI version of this software is available at <http://www.mrf-registration.net/>.

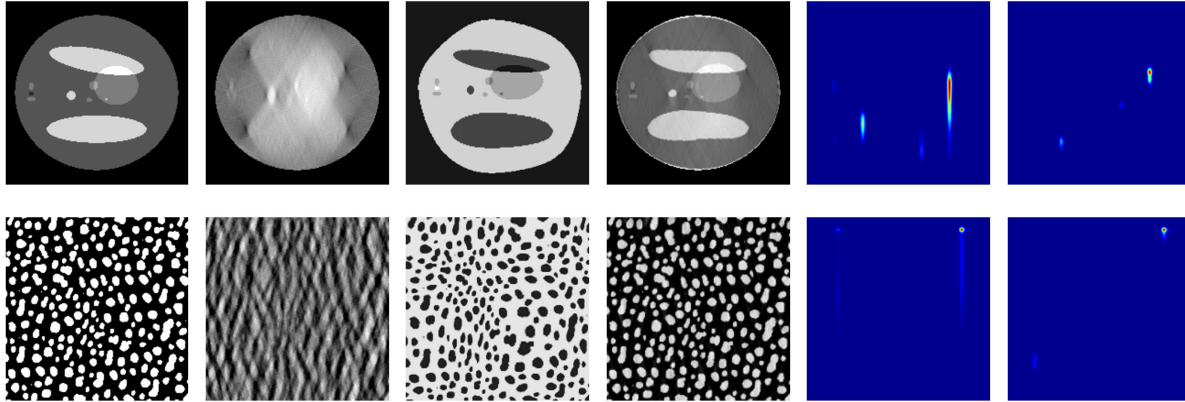


Figure 1. Reconstruction of attenuation maps from 16 simulated projections distributed evenly over $\pm 30^\circ$ and an unregistered anatomical prior. Top row: ellipse phantom. Bottom row: random blob phantom. Left to right: original, unregularized ML, prior, SRR, joint pdf by ML, joint pdf by SRR. The maximum misalignment is 8.5 pixels, compared to a total image size of 200x200.

3.1 Conclusions

We proposed a simultaneous reconstruction and registration algorithm that is capable of mitigating the data insufficiency problem of limited view tomography. We derived a cost function using Bayesian probability theory, and proposed an efficient approximation to the similarity metric for use in the reconstruction step, as standard information theoretic metrics were previously found to be ill-suited for regularizing limited view tomographic reconstructions. The particular approximation used was to consider the joint entropy of a single Gaussian approximation to the joint histogram and to minimize it. This yielded an objective function in x that was entirely quadratic in x , and hence allowed us to use standard optimization methods with fast iteration times and high convergence rates. We also noted that there is a tremendous amount of flexibility in the choice of similarity metrics, image interpolation models, and deformation field models. Hence there is a considerable scope for further optimization of these design choices in our future work. Finally, we note that the the proposed framework could also be applied to anatomical regularization in emission tomography.

References

1. J.T. Dobbins III & D.J. Godfrey. "Digital x-ray tomosynthesis: current state of the art and clinical potential." *Phys. Med. Biol.* **45**, pp. R65–R106, 2003.
2. Kak, A. C. & Slaney, M. *Principles of Computerized Tomographic Imaging*. Society of Industrial and Applied Mathematics, 2001.
3. B. Nett, J. Tang, S. Leng et al. "Tomosynthesis via total variation minimization reconstruction and prior image constrained compressed sensing (piccs) on a c-arm system." volume 6913, p. 69132D. SPIE, 2008.
4. Y. Mameuda & H. Kudo. "New anatomical-prior-based image reconstruction method for pet/spect." *NSS '07. IEEE* **6**, pp. 4142–4148, 2007.
5. S. Somayajula, E. Asma & R. Leahy. "Pet image reconstruction using anatomical information through mutual information based priors." *NSS '05. IEEE* **5**, pp. 2722–2726, 2005.
6. J. Nuyts. "The use of mutual information and joint entropy for anatomical priors in emission tomography." *Nuclear Science Symposium Conference Record, 2007. NSS '07. IEEE* **6**, pp. 4149–4154, 26 2007-Nov. 3 2007.
7. J. Tang, B. Tsui & A. Rahmim. "Bayesian pet image reconstruction incorporating anato-functional joint entropy." *ISBI 2008* pp. 1043–1046, May 2008.
8. D. Van de Sompel & M. Brady. "Robust Joint Entropy Regularization of Limited View Transmission Tomography using Gaussian Approximations to the Joint Histogram." In *Accepted for poster presentation at the 21st biennial International Conference on Information Processing in Medical Imaging (IPMI 09)*.
9. H. Erdogan & J.A. Fessler. "Accelerated monotonic algorithms for transmission tomography." In *ICIP (2)*, pp. 680–684. 1998.
10. B. Glocker, N. Komodakis, G. Tziritas et al. "Dense image registration through MRFs and efficient linear programming." *Medical Image Analysis* **12(6)**, pp. 731–741, 2008.